OPTOELECTRONICS AND ADVANCED MATERIALS – RAPID COMMUNICATIONS Vol. 4, No. 11, November 2010, p. 1685 - 1689

Synthesis and fluorescent properties of well-dispersed $Y_2O_3:Eu^{3+}$ nanocrystals

H. JIANG, H. WEI*
College of Chemistry and Biology, Beihua University, Jilin 132033, P. R. China

Uniform-sized and well-crystalline Eu^{3+} doped Y_2O_3 nanocrystals (NCs) have been successfully synthesized via a metal-oleate decomposition method using 1-octadecene as high boiling organic solvents. X-ray diffraction (XRD), field emission scanning electron microscopy (FE-SEM), transmission electron microscopy (TEM), Fourier transform infrared (FT-IR), photoluminescence (PL) and the kinetic decay were employed to characterize the samples. It was found that $Y_2O_3:Eu^{3+}$ nanocrystals can be indexed to cubic Y_2O_3 phase with high purity. The FE-SEM and TEM images reveal that the as-prepared $Y_2O_3:Eu^{3+}$ consists of uniform nanospheres with the mean particle size of 19 nm in a relatively narrow size distribution. The $Y_2O_3:Eu^{3+}$ nanocrystals exhibit strong luminescence upon ultraviolet excitation, suggesting its potential application in the fields of color displays and bioimaging.

(Received September 8, 2010; accepted November 10, 2010)

Keywords: Oleic acid, Luminescence, Y_2O_3, 1-octadecene

1. Introduction

During the past decades, the development of nanocrystals with well-defined and controllable shape and size has been extensively pursued, because the properties of these nanocrystals strongly depend on their geometrical factors such as morphology, dimensionality, and size [1–4]. For example, the color sharpness of semiconductor optical devices closely interrelates with the uniformity of the nanocrystals [5–7], and mono-dispersity of magnetic nanocrystals play a key role in the next-generation magnetic storage media [8]. Up to date, a number of strategies have been developed in manipulating the size and shape of various nanocrystals including semiconductors, metals, alloys, and metal oxides [9–12]. Among all the synthetic methods for the preparation of the high-crystalline and well-dispersed colloid nanocrystals, metal-organic based synthetic route has been proved a general strategy to synthesize shape-and size- controlled nanoparticles [10,13]. Due to the adsorption of surfactants onto the surfaces of these nanocrystals, the agglomeration of nanocrystals obtained by this method can be markedly avoided, which can effectively control the shape and size of as-prepared nanocrystals. Additionally, the nanocrystals that are capped by long chain alkyl hydrophobic groups can be well-dispersed in nonpolar solvents such as cyclohexane and chloroform to form a clear and stable colloidal solution.

Doping is a widely applied technological process in materials science for the fabrication of hybrid materials with desirable properties and functions. For rare earth based luminescent materials, doping is of fundamental importance in achieving and modifying the optical properties for the obtained materials. Currently, europium ions doped yttrium oxide ($Y_2O_3:Eu^{3+}$) has been proved one of the best red phosphors available due to its good luminescent properties, high quantum efficiency, short decay time, high melting point, and very high thermal conductivity [14–16]. During the past decade, various approaches have been developed for the fabrication of $Y_2O_3:Eu^{3+}$ particles with different shapes and dimensions, such as nanoparticles via combustion method [17], microemulsion [18], and chemical vapor technique [19]; nanotubes by a surfactant-induced assembly [20]; nanowires by template-assisted growth [21]; microspheres by hydrothermal process [22], and Pechini sol-gel process [23]. However, to the best of knowledge, metal–organic based decomposition synthetic route for the preparation of well-dispersed $Y_2O_3:Eu^{3+}$ nanocrystals has rarely reported.

Herein, we proposed the synthesis and luminescent properties of as-prepared $Y_2O_3:Eu^{3+}$ nanocrystals via a rare earth-oleate complex decomposition method using oleic acid and 1-octadecene as boiling solvent. The physicochemical properties of the as-prepared nanoparticles were well characterized by XRD, TEM, FT-IR, PL spectrum, respectively. The as-obtained nanocrystals capped by long chain oleic acid can be well-dispersed in nonpolar solvents (cyclohexane), and well distributed in a relatively narrow size distribution, which exhibit the characteristic emission of Eu^{3+} excited by ultraviolet irradiation.

2. Experimental details

2.1. Regents and materials

1-Octadecene and oleic acid were purchased from Sigma-Aldrich and used with further purification. Sodium oleate and rare earth (RE) oxides (Y_2O_3, Eu_2O_3, 99.99%) were obtained from Sinapharm Chemical Reagent Co., Ltd. (Shanghai, China). YCl_3 and $EuCl_3$ were prepared by dissolving the corresponding rare earth oxides in dilute hydrochloric acid at elevated temperature followed by evaporating the water under vacuum.

2.2. Synthesis of $Y_2O_3:Eu^{3+}$ nanocrystals

The rare earth-oleate complex was prepared via reacting rare earth chlorides and sodium oleate. In a typical process, 0.9275 g of YCl_3 (3.8 mmol), 0.0517 g of $EuCl_3$ (0.2 mmol), and 3.65 g of sodium oleate (12 mmol) was dissolved in a mixed solvent containing 8 ml ethanol, 6 ml distilled water and 14 ml hexane. The obtained solution was heated to 70 °C and maintained at this temperature for four hours. The solution was then separated using a separatory funnel. The upper organic layer containing yttrium (europium) oleate complex was separated and collected, washed with deionized water four times, and dried in an oven overnight at 80 °C to remove the water and hexane, resulting in the rare earth-oleate complex in a waxy solid form.

1 mmol of as-prepared yttrium (5 mol % europium) oleate complex was dissolved in a mixed solvent composed of 10 mL of oleaic acid and 10 mL of 1-octadecene in a three-neck flask. The mixture solution was heated to 100 °C and degassed at this temperature under Ar for 30 min. Subsequently, the solution was heated to 320 °C with a heating rate of 3.3 °C/min and maintained at this temperature for 1.5 h. Afterward, the solution was naturally cooled to room temperature and precipitated by excess ethanol. The formed precipitate was centrifuged and the upper supernatant was decanted. The isolated solid was then dispersed in cyclohexane.

2.3. Characterization

X-ray diffraction (XRD) was examined on a Rigaku-Dmax 2500 diffractometer using Cu Kα radiation (λ = 0.15405 nm). FE-SEM images were obtained on a field emission scanning electron microscope (FESEM, S4800, Hitachi) equipped with an energy-dispersive X-ray spectrum (EDS, JEOL JXA-840). Transmission electron microscope (TEM) and high-resolution transmission electron microscope (HRTEM) were performed on a FEI Tecnai G^2 S-Twin transmission electron microscope with a field emission gun operating at 200 kV. Fourier-Transform IR (FT-IR) spectra were measured on a Perkin-Elmer 580B IR spectrophotometer using KBr pellet technique. The excitation and emission spectra were obtained on a Hitachi F-4500 spectrofluorimeter equipped with a 150 W xenon lamp as the excitation source. Luminescence decay curves were obtained from a Lecroy Wave Runner 6100 Digital Oscilloscope (1 GHz) using a 250 nm laser (pulse width = 4 ns, gate = 50 ns) as the excitation source (Continuum Sunlite OPO). All the measurements were performed at room temperature.

3. Results and discussion

3.1. Phase identification

The phase purity and the composition of the as-prepared $Y_2O_3:Eu^{3+}$ nanocrystals were examined by the XRD analysis, as shown in Fig. 1a. Vertical bars (Fig. 1b) show the standard cubic bulk Y_2O_3 peak positions (JCPDS No. 88–1040). It can be seen that all the diffraction peaks can be well indexed to a cubic lattice (space group: Ia-3) of pure Y_2O_3. And no additional peaks for other impurities can be detected, indicating the high purity of the as-prepared product. The calculated lattice constant, a = 10.6061 Å, is well consistent with that a = 10.6017 Å from the standard card (JPCDS No. 88–1040). The slightly enhanced lattice constants can be due to the larger ion radius of the doped components. It should be noted that the diffraction peaks for the as-prepared sample show some broadening, exhibiting the nano-sized nature of the particles. The peak broadening can be used to calculate the crystallite size by the Scherrer formula, $D = 0.89\lambda/\beta\cos\theta$, where D is the average grain size, λ is the X-ray wavelength (0.15405 nm), and θ and β are the diffraction angle and full-width at half-maximum (FWHM), respectively. The average crystallite size is estimated to be 19.1 nm, which is much close to that observed from SEM and TEM images (see the next morphology part).

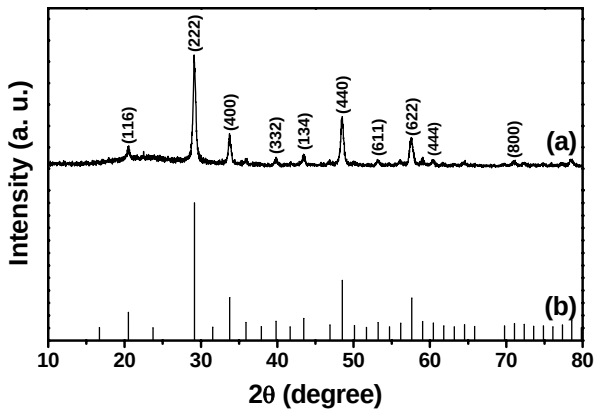

Fig. 1. XRD patterns of the as-prepared $Y_2O_3:Eu^{3+}$ nanocrystals (a), and the standard data for cubic Y_2O_3 phase (JCPDS 88-1040) (b).

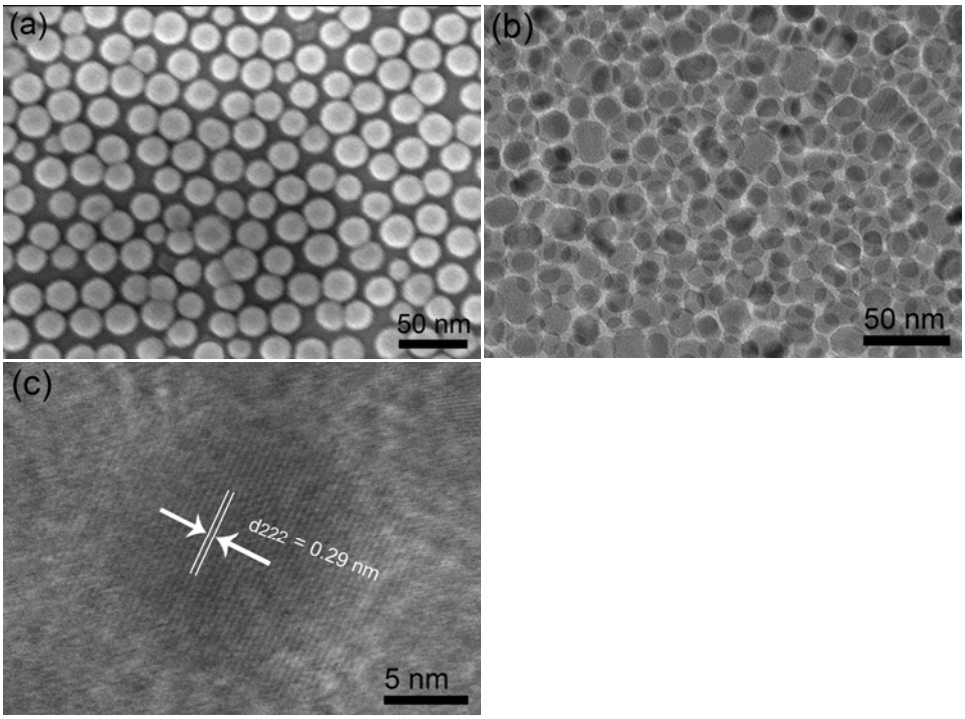

Fig. 2. FE-SEM (a), TEM (b), and HRTEM (c) images of the as-prepared $Y_2O_3:Eu^{3+}$ nanocrystals.

3.2. Morphology analysis

Oleic acid was used as the surfactant to control the size and shape of the $Y_2O_3:Eu^{3+}$ nanocrystals. Fig. 2 shows the FE-SEM, TEM images with low and high-resolution of as-prepared $Y_2O_3:Eu^{3+}$ nanocrystals, respectively. It can be seen from the FE-SEM image (Fig. 2a) that the as-prepared $Y_2O_3:Eu^{3+}$ consists of quasi mono-dispersed nanoparticles with a mean particle size of about 20 nm in a relatively narrow size distribution. The results are well consistent with the XRD analysis. The shape and size of as-prepared $Y_2O_3:Eu^{3+}$ in the TEM image (Fig. 2b) is much similar to the SEM result. Fig. 2c represents the typical HRTEM image of the as-prepared $Y_2O_3:Eu^{3+}$ nanocrystals. As shown, the obvious lattice fringes are apparent, indicating that the $Y_2O_3:Eu^{3+}$ nanocrystals possess high crystallinity. The inter-planar spacing (pointed by the arrows) of the $Y_2O_3:Eu^{3+}$ nanocrystals is determined to be about 0.29 nm, which is in accordance with the (222) facet distance (0.2915 nm) for bulk $Y_2O_3:Eu^{3+}$ phase.

3.3. Surface structure

FT-IR measurement was used to investigate the functional groups on the surface of the as-prepared $Y_2O_3:Eu^{3+}$ nanocrystals, as shown in Fig. 3. The broad absorption band at 3449 cm^{-1} can be ascribed to the stretching vibration of the hydroxyl group (–OH) of absorbed water molecules. The absorption peaks located at 1718, 1545 and 1463 cm^{-1} can be assigned to the stretching vibrations of COO^-. The sharp peaks at 2854 and 2925 cm^{-1} are associated with the symmetric and anti-symmetric stretch vibration of the $–CH_2$ group of the oleic acid. The shoulder 2959 cm^{-1} can be related with the anti-symmetric stretch of methyl. It can be deduced from the IR spectrum that the as-prepared $Y_2O_3:Eu^{3+}$ nanocrystals are capped by oleic acid molecules, which make it dissolve in cyclohexane based on their hydrophobic surface.

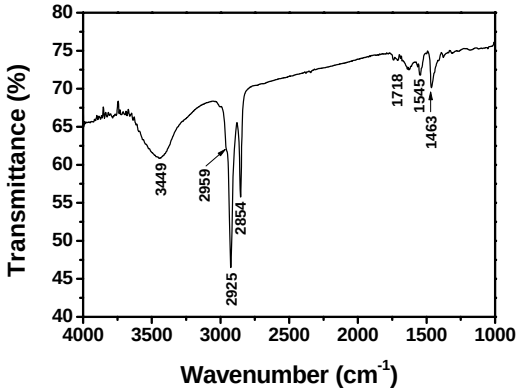

Fig. 3. FT-IR spectrum of the as-prepared $Y_2O_3:Eu$ nanocrystals.

3.4. Optical characterization

The photoluminescent (PL) properties of as-prepared Y_2O_3:Eu^{3+} nanocrystals were characterized by the excitation (left) and emission (right) spectra, as shown in Fig. 4. It can be seen that the well-shaped nanocrystals exhibit strong red emission centered at 612 nm, and the spectra properties are typical for the well-known Y_2O_3:Eu^{3+} phosphors [22,23]. The excitation spectrum (Fig. 4, left) is composed of a broad band with a maximum at 249 nm due to the charge-transfer band (CTB) between O^{2-} and Eu^{3+} ions. And f-f transition lines of the Eu^{3+} ions with very weak intensity can be detected in the longer wavelength region. Upon excitation into the CTB at 249 nm, the characteristic transition lines from the excited $^5D_0$ level of Eu^{3+} are obvious in the emission spectrum (Fig. 4, right). The locations of the emission lines with their assignments are labeled in the figure. The main characteristic peaks observed in the red region originate from $^5D_0 \rightarrow {}^7F_0$ (580 nm), $^5D_0 \rightarrow {}^7F_1$ (588 nm), $^5D_0 \rightarrow {}^7F_2$ (612 nm), and $^5D_0 \rightarrow {}^7F_3$ (649 nm), respectively. It is obvious that the emission spectrum is dominated by the hypersensitive red emission $^5D_0 \rightarrow {}^7F_2$ transition at 612 nm.

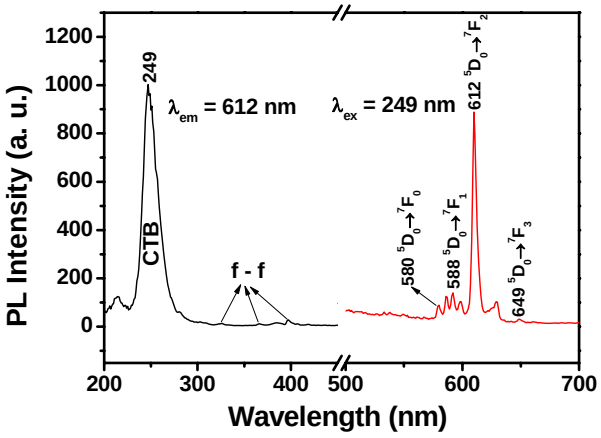

Fig. 4. The excitation (left) and emission (right) spectra of the as-prepared Y_2O_3:Eu nanocrystals.

The decay curve for the $^5D_0 \rightarrow {}^7F_2$ of Eu^{3+} in Y_2O_3:Eu^{3+} nanocrystals (λ_{ex} = 249 nm) is presented in Fig. 5. It can be seen that the decay curve can be well fitted into a single-exponential function as $I = A\ exp(-t/\tau)$ (A is the initial emission intensity at t = 0 and τ is the 1/e lifetime of the emission center), and the fitting parameters are given inside the figure. The calculated average lifetime are 1.09 ms for $^5D_0 \rightarrow {}^7F_2$ of Eu^{3+}, basically agreeing with the reported lifetime value for Eu^{3+} doped Y_2O_3 [22,23].

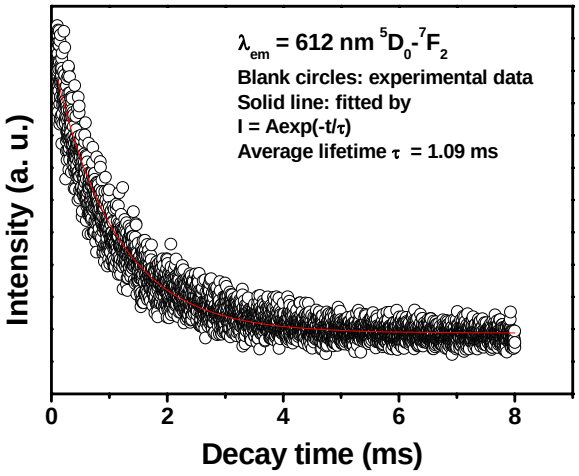

Fig. 5. The decay time of the as-prepared Y_2O_3:Eu^{3+} nanocrystals.

4. Conclusions

In summary, we reported the synthesis of the well-dispersed cubic Y_2O_3:Eu^{3+} nanocrystals with quasi-spherical shape in a relatively narrow size distribution. The as-synthesized Y_2O_3:Eu^{3+} nanocrystals are highly crystalline and well-dispersed in cyclohexane to form a clear and stable colloidal solution, which exhibit strong red emission upon ultraviolet excitation. The as-prepared product shows great promising applications as biolabeling, displays and other optical applications.

References

[1] X. Peng, L. Manna, W. Yang, J. Wickham, E. Scher, A. Kadavanich, A. P. Alivisatos, Nature **404**, 59 (2000).
[2] J. Y. Lao, J. G. Wen, Z. F. Ren, Nano Lett. **2**, 1287 (2002).
[3] H. Cölfen, S. Mann, Angew. Chem. Int. Ed. **42**, 2350 (2003).
[4] Z. W. Quan, J. Yang, P. P. Yang, Z. L. Wang, C. X. Li, J. Lin, Cryst. Growth Des. **8**, 200 (2000).
[5] P. Alivisatos, Science **271**, 933 (1996).
[6] M. Nirmal, L. Brus, Acc. Chem. Res. **32**, 407 (1999).
[7] C. B. Murray, C. R. Kagan, M. G. Bawendi, Annu. Rev. Mater. Sci. **30**, 545 (2000).
[8] S. Sun, C. B. Murray, D. Weller, L. Folks, A. Moser, Science **287**, 1989 (2000).
[9] J. J. Li, Y. A. Wang, W. Z. Guo, J. C. Keay, T. D. Mishima, M. B. Johnson, X. G. Peng, J. Am. Chem. Soc. **125**, 13567 (2003).
[10] Y. G. Sun, Y. N. Xia, Science **298**, 2176 (2002).
[11] C. Desvaux, C. Amiens, P. Fejes, P. Renaud, M. Respaud, P. Lecante, E. Snoeck, B. Chaudret, Nat. Mater. **4**, 750 (2005).

[12] T. S. Ahmadi, Z. L. Wang, T. C. Green, A. Henglein, M. A. Elsayed, Science **272**, 1924 (1996).
[13] T. Hyeon, S. S. Lee, J. Park, Y. Chung, H. B. Na, J. Am. Chem. Soc. **123**, 12798 (2001).
[14] W. N. Wang, W. Widiyastuti, T. Ogi, I. W. Lenggoro, K. Okuyama, Chem. Mater. **19**, 1723 (2007).
[15] Y. Mao, J. Y. Huang, R. Ostroumov, K. L. Wang, J. P. Chang, J. Phys. Chem. C **112**, 2278 (2008).
[16] S. C. Cho, H. S. Uhm, C. U. Bang, D. K. Lee, C. S. Han, Thin Solid Films **517**, 4052 (2009).
[17] Z. M. Qi, C. S. Shi, Appl. Phys. Lett. **81**, 2857 (2002).
[18] Q. Pang, J. Shi, Y. Liu, Mater. Sci. Eng. B **103**, 57 (2003).
[19] A. Konrad, T. Fries, A. Gahn, J. Appl. Phys. **86**, 3129 (1999).
[20] C. F. Wu, W. P. Qin, G. S. Qin, Appl. Phys. Lett. **82**, 520 (2003).
[21] J. L. Zhang, G. Y. Hong, J. Solid State Chem. **177**, 1292 (2004).
[22] J. Yang, Z. W. Quan, D. Y. Kong, X. M. Liu, J. Lin, Cryst. Growth Des., **4**, 7 (2007).
[23] H. Wang, C. K. Lin, X. M. Liu, J. Lin, Appl. Phys. Lett. **87**, 181907 (2005).

* Corresponding author: weihong750105@sina.com